



Porous carbon nanospheres with high EDLC capacitance

Gang Li^a, Xiaozhuan Gao^a, Kaiying Wang^{a,b,*}, Zaijun Cheng^{c,**}



^a MicroNano System Research Center, College of Information and Computer & Key Lab of Advanced Transducers and Intelligent Control System (Ministry of Education), Taiyuan University of Technology, Taiyuan 030024, China

^b Department of Microsystems Technology-IMS, University of Southeast Norway, Horten 3184, Norway

^c School of Optoelectronic and Communication Engineering, Xiamen University of Technology, Xiamen 361024, China

ARTICLE INFO

Keywords:

Glucose
Hollow carbon nanospheres
KOH activation
EDLCs

ABSTRACT

This paper reports on the fabrication and electrochemical properties of porous carbon nanospheres, which have been prepared by the hydrothermal carbonization of natural glucose and subsequent activation of potassium hydroxide (KOH). Porous nanospheres with high bulk porosity and partial graphitization are obtained by the optimization of mass ratio (KOH: hydrochar). The optimal of specific surface area reaches $1563\text{ m}^2/\text{g}$ with an average diameter of 3.64 nm. The maximum of specific capacitance of the activated carbon nanospheres is 207 F/g at a current density of 0.5 A/g, high rate capability (181 F/g at a current density of 10 A/g) and cycling stability (capacitance retention of nearly 96.7% over 1000 cycles). The high-conductive porous carbon nanosphere material with low microporosity and blind porosity might be a potential material for electrochemical double-layer capacitors (EDLCs).

1. Introduction

Electrochemical double-layer capacitors (EDLCs), usually also known as supercapacitors, have attracted considerable attention as one of energy storage devices because of their short charging time, high power density, low cost, and long life cycles [1–4]. Porous carbons as electrode materials are promising in EDLCs because they can provide high specific surface area, excellent conductivity, high physiochemical stability, and relatively low cost-effectiveness [4,5]. Generally, the approaches of pyrolysis and hydrothermal carbonization (HTC) are used to synthesis porous carbon. The HTC technology is a preferred process, which can prepare spherical carbon materials from natural precursors. The process does not use expensive organic solvents or catalysts and only requires low processing temperature ($< 300^\circ\text{C}$) [5–7].

Recently, glucose as a carbon source has attracted growing interests because it is abundant, commercially available, eco-friendly and natural renewable. However, the electrochemical performance of the HTC processed glucose is rather poor for commercial EDLC application. Therefore, many approaches have been attempted to improve the capacitance performance of the glucose-derived porous carbon materials. For instance, Qiu et al. reported a method to synthesize phosphorus- and nitrogen-co-doped glucose-derived microporous carbons, and the

specific capacitance can reach 183.8 F/g at a current density of 0.05 A/g in 6 M KOH electrolyte [8]. Zhou et al. used glucose and human hair as carbon precursors to synthesis porous carbon, which displayed a specific capacitance of 264 F/g at a current density of 0.25 A/g in 6 M KOH electrolyte [9]. Dong et al. reported nitrogen-doped activated carbon sheet with a specific capacitance of 312 F/g at a current density of 0.5 A/g in 6 M KOH aqueous electrolyte [1]. Hu et al. combined carbon nanotubes and glucose to synthesis porous carbon, which exhibited a specific capacitance of 210 F/g at a current density of 0.5 A/g in 6 M KOH aqueous electrolyte [10]. However, the HTC glucose-derived EDLCs show high fraction of unavailable micropores ($< 2\text{ nm}$) [11,12], blindpores [13,14] (with closed ends), which cannot provide enough voids for ion diffusion and transportation and limit their capacitance properties. Thus, optimizing the pore structure to obtain highly effective surface area is an effective strategy to improve the electrochemical performance of carbon electrode materials [15,16]. Furthermore, high electrical conductivity, which is related to graphitization of carbon, is also desired for carbon electrode materials [17]. So far, to our best knowledge, tuning the pore structure and graphitization of the HTC processed glucose to form highly-conductive, porous nanospheres are less reported for exploring EDLC applications.

In this work, a facile and scalable HTC method has been applied for synthesizing carbon nanospheres, and KOH chemical activation is

* Correspondence to: K. Wang, MicroNano System Research Center, College of Information and Computer & Key Lab of Advanced Transducers and Intelligent Control System (Ministry of Education), Taiyuan University of Technology, Taiyuan 030024, China.

** Correspondence to: Z.J. Cheng, School of Optoelectronic and Communication Engineering, Xiamen University of Technology, Xiamen 361024, China

E-mail addresses: Kaiying.Wang@usn.no (K. Wang), 2011111002@xmut.edu.cn (Z. Cheng).

subsequently used to tailor the pore texture of hydrochar for producing highly porous carbon nanospheres. The morphology, pore structure and electrical conductivity of the as-prepared hydrochar are strongly dependent on the KOH activation process, and are investigated by Scanning Electron Microscopy (SEM), Raman Spectra and X-ray diffraction (XRD). The electrochemical performances of optimized porous nanospheres are further evaluated for potential EDLC applications.

2. Experimental

2.1. Synthesis and activation of hydrothermal carbon

All chemicals and reagents in this study were of analytical grade without further purification, and all glassware was dried at 80 °C for several hours. Carbon nanospheres were prepared by an HTC process of the glucose. In the experiments, glucose (5 g) and deionized water (50 ml) were added to a 70 ml Teflon lined stainless autoclave. The autoclave was heated to 260 °C and kept for 12 h, and left to cool down to room temperature. The as-prepared hydrochar was then collected and washed in deionized water and dilute hydrochloric acid and vacuum-dried at 80 °C overnight prior to use. Chemical activation was then carried out to tailor the pore texture with KOH nanoparticles, which were mixed with the prepared hydrochar in an agate mortar for a well-proportioned mix. The mass ratios of hydrochar and KOH are fixed at 1:0, 1:1, 1:2, 1:3 and 1:4. The chemical activation was performed by heating the mixture from room temperature to 800 °C for 2 h under nitrogen (purity, 99.99%) gas. After such activation, the sample was sequentially washed with 1 mol/L HCl solution to remove inorganic salts and then with distilled water until a neutral pH was achieved. Finally, the activated hydrochar was additionally dried at 120 °C overnight. According to the activation mass ratios, these as-prepared samples were labeled as AC, AC-1, AC-2, AC-3 and AC-4, respectively.

2.2. Preparation and characterization

As-prepared activated carbon nanospheres were mixed with the polyvinylidene fluoride (PVDF) binder, conductive powder (acetylene black) in a mass ratio of 8:1:1 and then dispersed in the *N*-methyl-2-pyrrolidone (NMP) solvent to form a slurry. The resulting slurry was

then pasted onto Ni foam and dried at 120 °C in a vacuum oven to form an electrode. Mass loading of the active electrode material was about 2 mg/cm². Morphology, crystallographic structure and electrical conductivity of the activated hydrochar were examined by scanning electron microscopy (SEM, SU-3500), X-ray diffraction (XRD) system. Energy Dispersive X-Ray (EDX) spectra was observed by IXRF with a resolution of 123 eV. A raman spectrum was collected on a Jobin-Yvon LabRam HR800 Raman spectroscope.

2.3. Electrochemical measurements

All electrochemical performance was measured in a typical three-electrode setup: Ni foam coated with carbon nanospheres as working electrode, platinum foil and Ag/AgCl electrode as counter and reference electrodes. Cyclic voltammetry (CV), galvanostatic charge/discharge (GCD) and electrochemical impedance spectroscopy (EIS) were performed in 1 mol/L Na₂SO₄ aqueous solution using a ZAHNER-PP211 electrochemical workstation. CV curves were measured under a potential range from –0.1 to 0.9 V (vs. Ag/AgCl) at various scan rates. GCD curves were measured at different current densities of 0.5, 1, 2, 3, 5 and 10 Ag^{−1}, and EIS curves were measured in the frequency range from 10 MHz to 100 KHz with an AC perturbation of 5 mV at open circuit potential.

3. Results and discussions

3.1. Morphology characterization

Morphology of the KOH-activated hydrochar was characterized by SEM and presented in Fig. 1. As shown in Fig. 1(a), the interconnected carbon nanospheres with diameters in the range of 450–500 nm were obtained through hydrothermal carbonization of glucose. This type of carbon nanospheres is normally observed for the carbons derived from polysaccharide biomass such as glucose, sucrose, starch and cellulose. However, solid carbon nanospheres are difficult to be wet with electrolyte due to lacking of suitable pores that offer sufficient reservoirs for electrolyte and lead to low capacitance performance. The pores on the surface of carbon nanospheres can be enlarged when the KOH/hydrochar mass ratio increases. By increasing KOH/hydrochar mass ratio

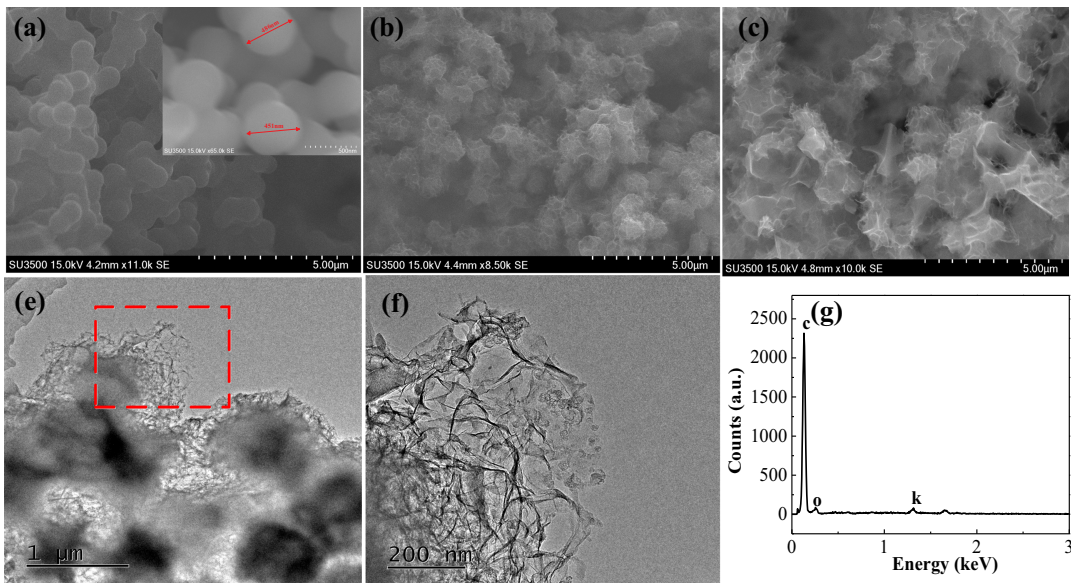


Fig. 1. SEM images of as-prepared (a) AC, (b) AC-3, (c) AC-4; (e) TEM image of AC-3, (d) high magnification graph of red box section in panel e, (g) EDX spectra of AC-3. (For interpretation of the references to color in this figure legend, the reader is referred to the web version of this article.)

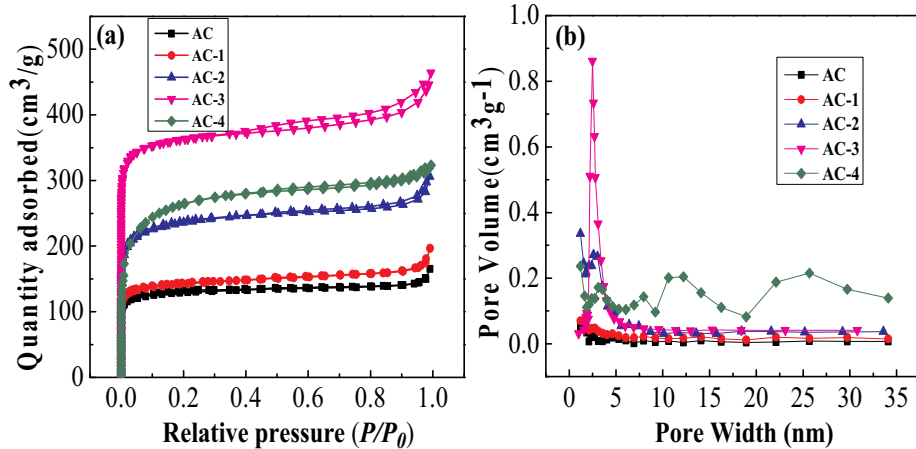


Fig. 2. (a) Nitrogen adsorption–desorption isotherms and (b) pore size distribution for as-prepared AC, AC-1, AC-2, AC-3, and AC-4, respectively.

equal to 3, the AC-3 exhibits a clear porous nano-spherical shape as shown in Fig. 1(b). The pore structure of AC-3 can be clearly observed from the TEM image (Fig. 1(d)) and higher magnification TEM image (Fig. 1(e)), which shows a well-controlled, porous carbon nanosphere structure. However, the spherical morphology is partially distorted when the mass ratio of KOH/hydrochar was increased to 4 as shown in Fig. 1(c) because the excessive KOH will break the skeleton of the carbon structure and further produced some macropores, which may lead to a decrease in electrochemical performance. The EDX spectra (Fig. 1(f)) show that the major component is element carbon.

Nitrogen adsorption desorption test is further used to characterize the specific surface area and pore size distribution as shown in Fig. 2. Following the classification of International Union of Pure and Applied Chemistry (IUPAC), all samples exhibit a typical mesoporous structure material because they display a typical IV isotherm with type H2 hysteresis loop at the relative pressure range of 0.5–1.0, shown in Fig. 2(a). Detailed information of all carbon samples such as specific surface area (S_{BET}), total pore volume (V_{total}) and average pore diameter (D_p) are listed in Table 1 below. Specially, AC-3 exhibits the highest specific surface area among all samples. The specific surface area of AC-3 estimated by the BET method is 1563 m²/g, which is much higher than that of other samples and the corresponding reference data (i.e. 1036.7 m²/g [5], 1104 m²/g [9]). Furthermore, pore size distribution (PSD) is determined by Barret-Joyner-Halenda (BJH) on the experiment of nitrogen sorption isotherms (Fig. 2(b)). Among all samples, AC-3 also exhibits an excellent PSD result, which clearly shows a suitable pore size ranges from 2.4 to 5.0 nm with the average pore size of 3.64 nm and large pore volume 0.73 m³/g.

3.2. XRD and Raman analysis

Fig. 3(a) shows the XRD patterns of different activated samples. All carbon samples exhibit similar crystalline structures with two broad and weak diffraction peaks centered at $2\theta = 22^\circ$ and 43° , which

correspond, respectively, to the (002) and (100) diffraction planes of hexagonal graphite (JCPDS no.41–1487) [18,19]. A broad peak of the (002) reflection between 15° and 30° suggests that the crystalline structure is disordered [20]. The weak peaks around 43° are indexed to the (100) diffraction peak of graphitic structures in sp² carbon materials, suggesting that the carbon material is slightly graphitized [13]. The interlayer spacing of the AC, AC-1, AC-2, AC-3, and AC-4 samples are 0.395, 0.382, 0.376, 0.361, 0.373 nm, which are calculated by the Bragg equation [19] based on the (002) peak $2dsin\theta = n\lambda$. It can be seen that the interlayer spacing of porous carbon can be decreased by KOH activation.

Fig. 3(b) shows the Raman spectra of the carbon samples activated at different mass ratios. The Raman spectra of all carbon samples display a D peak (signal of the defect- or disorder-induced scattering) at 1350 cm⁻¹ and a G peak (signal of the vibration of sp²-bonded carbon atoms) at 1590 cm⁻¹. The D peak is associated with the vibrations of carbon atoms with dangling bonds in plane terminations of the disordered graphite from defects and disorders of the structures of carbon materials [21–23]. The G peak is attributed to the phonon mode with an E_{2g} symmetry of graphite and the vibration of sp² hybridized carbon atoms in a 2D hexagonal lattice [23]. The modulation peak at 1100 cm⁻¹–1200 cm⁻¹ indicates that amorphous component of the material was possibly caused by lattice polarization. The position, intensity, and broadening of the D peak (relative to G peak) depend on the nature of impurities and functional groups and the type of disorder [24]. As shown in Fig. 2(b), the highest intensity of the D peak suggests a high degree of structural disorder in AC-3 [24]. The intensity ratio of D-peak to G-peak (I_D/I_G) depends on the graphitization of carbon materials, and the lower I_D/I_G value will lead a higher graphitization degree in carbon materials [25]. The I_D/I_G of AC, AC-1, AC-2, AC-3 and AC-4 is calculated to be 0.932, 0.929, 0.915, 0.91 and 0.921, respectively, suggesting that graphitization can be optimized by KOH activation. It can be seen that the graphitization of AC-3 is the highest one in all carbon samples. Thus, the analysis of Raman spectra concurs with the XRD results.

3.3. Electrochemical test

Typical CV measurements are performed to determine the electrochemical properties of the carbon samples. Fig. 4(a) shows the CV characteristics of all carbon samples under the sweeping potential from -0.1 to -0.9 V (vs. Ag/AgCl reference electrode) at a scan rate of 100 mV/s. All CV plots exhibit a quasi-rectangular shape of a typical EDLC behavior. However, for all carbon samples the rectangular CV curves tend to be triangular shape at high potentials (0.9 V) and low potentials (-0.1 V) due to the sieving effect of electrolyte ions [26].

Table 1

Nitrogen adsorption desorption test for all carbon samples.

Samples	S_{BET} (m ² /g)	V_{total} (m ³ /g)	D_p (nm)
AC	698	0.3314	1.85
AC-1	765	0.3803	1.98
AC-2	1054	0.5781	2.03
AC-3	1563	0.7301	3.64
AC-4	1089	0.6063	2.05

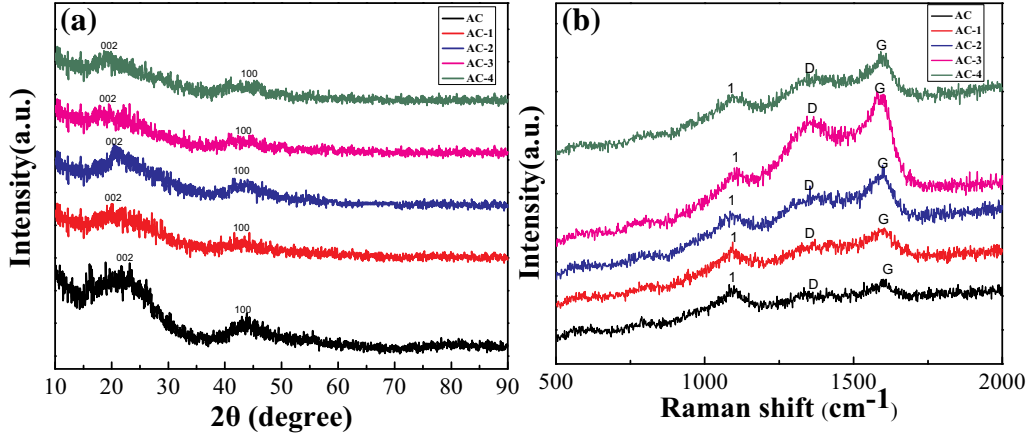


Fig. 3. (a) XRD patterns and (b) Raman spectra of as-prepared AC, AC-1, AC-2, AC-3, and AC-4, respectively.

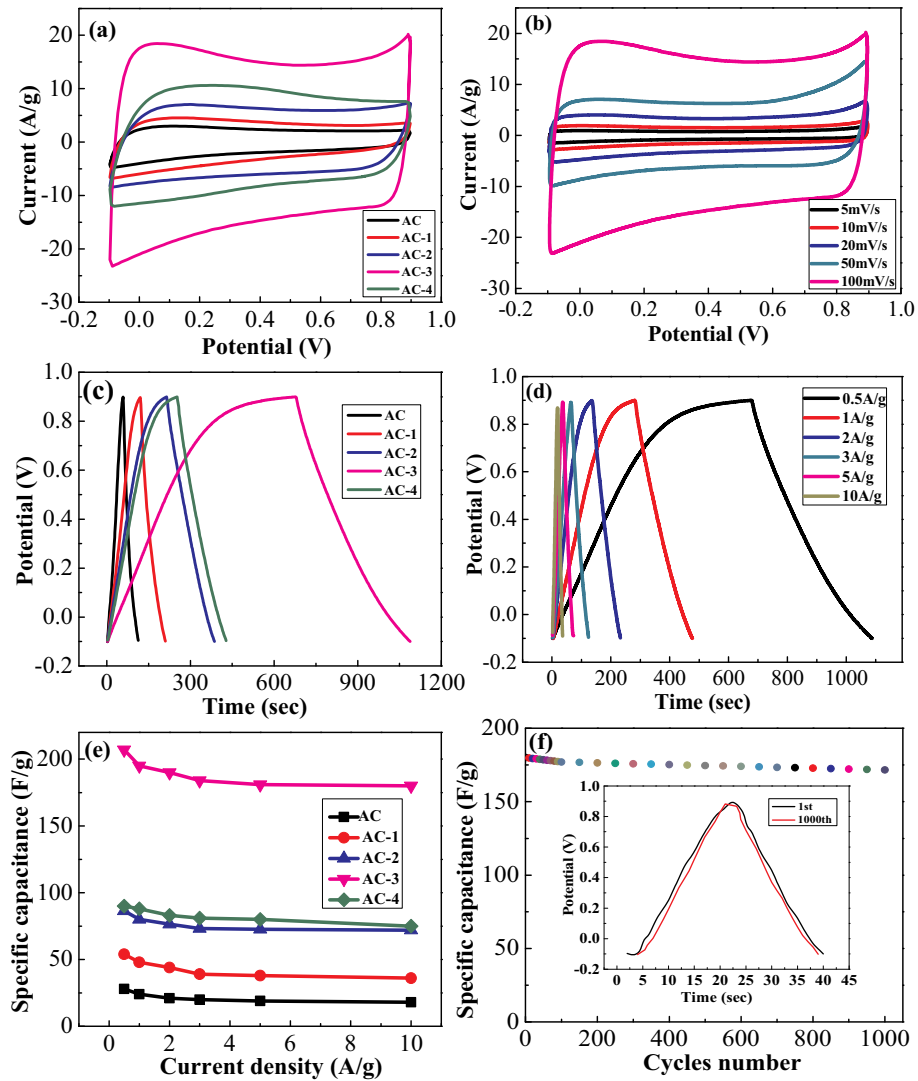


Fig. 4. (a) C-V curves of as-prepared AC, AC-1, AC-2, AC-3, and AC-4, respectively measured at a scan rate of 100 mV/s; (b) C-V curves of AC-3 respectively measured at different scan rates from 5 mV/s to 100 mV/s; (c) Charge-discharge curves of as-prepared AC, AC-1, AC-2, AC-3, and AC-4, respectively measured at the current density of 0.5 A/g; (d) C-V curves of AC-3 respectively measured current densities from 0.5 A/g to 10 A/g; (e) Specific capacitance of all carbon samples as a function of current densities; (f) Cycling stability of AC-3 at a current density of 10 A/g for 1000 cycles.

The specific capacitance is proportional to the covered areas of CV profile at same scan rate and potential window [22]. With the increasing KOH/carbon mass ratio, the specific capacitance firstly increases and then decreases, and the highest one is obviously found in AC-3. To further evaluate the rate capability of AC-3, CV tests are performed at different scan rates from 5 mV/s to 100 mV/s as shown in Fig. 4(b). The symmetry of CV curves decreases with the increase of scan rate, because the electrolyte ions do not easily diffuse into the inner channel of the carbon material at high scan rates and further cause electrochemical and ion concentration polarization. This will lead to a decrease of electric double-layer capacitance and the utilization of specific surface area of the electrode material [19].

Fig. 4(c) shows the GCD curves of all carbon samples measured at a current density of 0.5 A/g within a cell potential region from −0.1 to 0.9 V. Clearly, all GCD curves are almost linear and seem like isosceles triangles, indicating that the carbon samples have excellent electrochemical reversibility. Moreover, the iR drops on all curves are similar but not obvious, indicating low overall resistance and excellent power characteristics. The longest charge and discharge time take place in AC-3, which has the highest specific capacitance among all samples. Fig. 4(d) shows the GCD curves of AC-3 at the increasing current density from 0.5 A/g to 10 A/g. The charge and discharge time decreases with the increase of scan rate since a higher current density will lead to a lower specific capacitance. As described in CV curves, one possible reason is that the electrolyte ions have sufficient time to diffuse into the inner channel of the carbon materials to absorb more charges at low current density. According to the discharge curves at different current densities, the corresponding specific capacitance can be calculated by

$$C = \frac{i \times \Delta t}{m \times \Delta V} \quad (1)$$

where i is discharge current (A), Δt is discharge time (s), ΔV is the potential window (V), and m is the mass of the electrode materials (g).

Fig. 4(e) presents the corresponding specific capacitance at different current densities for all carbon samples. The specific capacitances of carbon samples are calculated to be 28 F/g, 54 F/g, 86 F/g, 207 F/g and 90 F/g at the current density of 0.5 A/g, respectively. The sample AC-3 exhibits high-level capability because the specific capacitance slightly decreases from 207 F/g at low current density of 0.5 A/g to 161 F/g at high current density of 10 A/g.

Cycling stability is another critical factor for the application of supercapacitor electrodes [27]. Fig. 4(f) shows the cycling stability of AC-3 by repeating galvanostatic charge-discharge measurements at a constant current density of 10 A/g for 1000 cycles. The sample AC-3 demonstrates an excellent cycling stability because the capacitance still remains ~96.7% after 1000 cycles. Furthermore, it is worth noting that the charge-discharge curves still exhibit nearly triangular forms after 1000 cycles and show stable performance and a good charge characteristic. The excellent cycling stability is attributed to the appropriate porosity and slight graphitization degree of AC-3 [22].

Table 2

Equivalent circuit parameters obtained by fitting program.

Sample	R_s (Ω)	R_p (Ω)	R_{CT} (Ω)	C_{DL} (μF)	W_O ($\Omega^{-1/2}$)	C_F (F)
AC	1.604	2.779	1.175	15,490	1.129	0.7361
AC-1	1.435	2.239	0.8046	2919	0.4805	0.1644
AC-2	0.952	1.669	0.7175	2387	0.3735	0.1387
AC-3	0.809	1.506	0.697	1454	0.3432	0.09055
AC-4	1.108	1.889	0.7806	2775	0.3744	0.1708

C_{DL} : double layer capacitance, W_O : Warburg diffusion element, C_F : Faradic capacitance; R_s : calculated from the point of intersection with the x-axis in the high frequency region; R_p : calculated from the point of intersection with the x-axis from medium frequency region; R_{CT} : diameter of the semicircle at high frequency region (R_p-R_s).

3.3.1. EIS

The electrochemical impedance spectroscopy (EIS) analysis is one method of investigating electrochemical behavior of electrode materials in terms of the electrical resistance and ion transport behaviors. To elaborate on the properties of conductivity and ion diffusion at electrode/electrolyte interface [28,29], the impedance spectra of all carbon samples have been measured in the frequency range of 10 MHz to 100 kHz at the potentials from −0.1 V to 0.9 V as shown in Fig. 5(a). Nyquist plots of all samples show similar shapes, which comprise a small arc in the high frequency region, a nearly straight line with a 45° slope in the medium frequency region and a nearly vertical line in the low frequency region. Clearly, the impedance response is a typical capacitive behavior of EDLCs electrodes.

The arc part is related to the charge transfer kinetics between the carbon materials, and corresponds to the internal or equivalent series resistance (ESR, R_s) of the electrode. The ESR of the carbon samples is 1.604 Ω , 1.435 Ω , 0.952 Ω , 0.809 Ω and 1.108 Ω in Table 2. The lowest R_s is from AC-3 since the carbon sample has the best conductivity [30]. The section of the straight line with a 45° slope is related to charge transfer resistance (Warburg resistance, R_p) at the electrode-electrolyte interface, and corresponds to the length of the Warburg-type line. The R_p are 2.779 Ω , 2.239 Ω , 1.669 Ω , 1.506 Ω and 1.889 Ω in Table 2. The lowest R_p also takes place in AC-3, indicating the carbon sample has the fastest diffusion rate [30]. The vertical line is related to charge transfer resistance (R_{CT}) within the electrode structure and corresponds to capacitive behavior. The R_{CT} are 1.175 Ω , 0.846, 0.7175 Ω , 0.697 Ω , and 0.7806 Ω in Table 2. The lowest R_{CT} also appears in AC-3, indicating the activated carbon sample with KOH/hydrochar mass ratio of 3 behaves more closely as an ideal capacitor due to the well-developed porosity after the KOH activation.

Ragone plots, as an efficient way to evaluate the capacitive performance of supercapacitors, have been used to characterize our electrode material. To characterize the operational performance, the energy density at different average power density (P) was calculated from the charge and discharge data at different current densities according to the

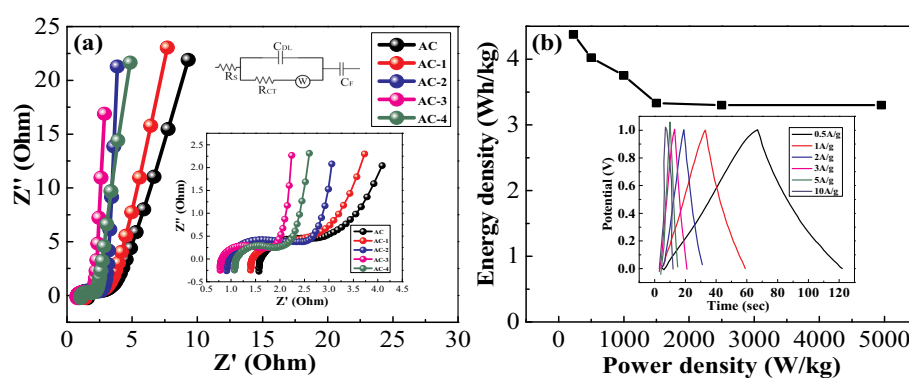


Fig. 5. (a) Nyquist plots measured in the range of frequency from 10 MHz to 100 kHz and (b) Ragone plots related to energy and power densities of as-prepared AC-3.

following equations:

$$E = \frac{1}{2}CV^2 \quad (2)$$

$$P = \frac{E}{t} \quad (3)$$

where E , C , P and t are the average energy density (Wh/kg), specific gravimetric capacitance (F/g), average power density (W/kg) and discharge time (s), respectively. Ragone plots of activated carbon under different scan rates are shown in Fig. 5(b). It can be seen that the AC-3 exhibits far higher electrochemical performances in comparison with other samples. For example, the energy density and power density of AC-3 reach 4.375 Wh/kg and 228.84 W/kg at a current density of 0.5 Ag⁻¹, respectively, and still remain 3.3 Wh/kg with the power density of 4.95 kW/kg at a high current density of 10 Ag⁻¹. The superior electrochemical performances of the AC-3 electrode are attributed to the numerous mesoporous, which can offer short ion diffusion lengths, facilitating the fast diffusion and transport of electrolyte ions during charge/discharge process.

4. Conclusions

In conclusion, natural glucose was used to synthesize carbon nanospheres by the HTC method. The best-activated hydrochar with good porosity and graphitization have been obtained with subsequent process of KOH/carbon mass ratio of 3.0. The optimized activated carbon nanospheres exhibit a high specific surface area (1563 m²/g), narrow PSD range (from 2.4 to 5.0 nm with average diameter of 3.64 nm), high specific capacitance (207 F/g at a current density of 0.5 A/g), excellent rate capability (181 F/g at a current density of 10 A/g) and good cycling stability (capacitance retention of nearly 98% over 1000 cycles). The EIS tests confirm the best-activated hydrochar with low R_s (0.809 Ω), R_p (1.506 Ω) and R_{CT} (0.697 Ω) behaves more closely as an ideal capacitor.

Acknowledgments

This research was supported by the National Natural Science Foundation of China (61504113, 61674113, 51622507, and 61471255), Natural Science Foundation of Shanxi Province, China (2016011040), Natural Science Foundation of Fujian Province, China (2018J01567) and Scientific and Technological Innovation Programs of Higher Education Institutions in Shanxi Province, China (2016138). The author KW acknowledged financial support from the Norwegian Research Council-FRINATEK programme (231416/F20). We appreciated the kind help from Asst. Prof. Richard Nelson for proofreading.

References

- [1] Y.L. Wang, H.Q. Xuan, G.X. Lin, F. Wang, Z. Chen, X.P. Dong, A melamine-assisted chemical blowing synthesis of N-doped activated carbon sheets for supercapacitor application, *J. Power Sources* 319 (2016) 262–270.
- [2] Y.Q. Zhao, M. Lu, P.Y. Tao, Y.J. Zhang, X.T. Gong, Z. Yang, G.Q. Zhang, H.L. Li, Hierarchically porous and heteroatom doped carbon derived from tobacco rods for supercapacitors, *J. Power Sources* 307 (2016) 391–400.
- [3] L. Miao, D.Z. Zhu, M.X. Liu, H. Duan, Z.W. Wang, Y.K. Lv, W. Xiong, Q.J. Zhu, L.C. Li, X.L. Chai, L.H. Gan, Cooking carbon with protic salt: nitrogen and sulfur self-doped porous carbon nanosheets for supercapacitors, *Chem. Eng. J.* 347 (2018) 233–242.
- [4] L. Miao, D.Z. Zhu, Y.H. Zhao, M.X. Liu, H. Duan, W. Xiong, Q.J. Zhu, L.C. Li, Y.K. Lv, L.H. Gan, Design of carbon materials with ultramicro-, supermicro- and mesopores using solvent- and self-template strategy for supercapacitors, *Microporous Mesoporous Mater.* 253 (2017) 1–9.
- [5] Y.Z. Wang, Y. Liu, W. Liu, G.X. Zhang, G.W. Liu, H.Y. Chen, J.L. Yang, Large-scale synthesis of highly porous carbon nanosheets for supercapacitor electrodes, *J. Alloys Compd.* 667 (2016) 105–111.
- [6] Y.P. Zhu, N. Li, T. Lv, Y. Yao, H.N. Peng, J. Shi, S.K. Cao, T. Chen, Ag-doped PEDOT:PSS/CNT composites for thin-film all-solid-state supercapacitors with a stretchability of 480%, *J. Mater. Chem. A* 6 (2018) 941–947.
- [7] L. Miao, D.Z. Zhu, M.X. Liu, H. Duan, Z.W. Wang, Y.K. Lv, W. Xiong, Q.J. Zhu, L.C. Li, X.L. Chai, L.H. Gan, N, S co-doped hierarchical porous carbon rods derived from protic salt: facile synthesis for high energy density supercapacitors, *Electrochim. Acta* 274 (2018) 378–388.
- [8] C.L. Wang, Y. Zhou, L. Sun, P. Wan, X. Zhang, J.S. Qiu, Sustainable synthesis of phosphorus- and nitrogen-co-doped porous carbons with tunable surface properties for supercapacitors, *J. Power Sources* 239 (2013) 81–88.
- [9] W.J. Si, J. Zhou, S.M. Zhang, S.J. Li, W. Xing, S.P. Zhuo, Tunable N-doped or dual N, S-doped activated hydrothermal carbons derived from human hair and glucose for supercapacitor applications, *Electrochim. Acta* 107 (2013) 397–405.
- [10] F. Yu, L. Sun, C.G. Tian, H.B. Lin, The AMWCNTs supported porous nanocarbon composites for high-performance supercapacitor, *Mater. Res. Bull.* 48 (2013) 4491–4498.
- [11] L.H. Yin, Y. Chen, D. Li, X.Q. Zhao, B. Hou, B.K. Cao, 3-Dimensional hierarchical porous activated carbon derived from coconut fibers with high-rate performance for symmetric supercapacitors, *Mater. Des.* 111 (2016) 44–50.
- [12] M.J. Zhi, F. Yang, F.K. Meng, M.Q. Li, A. Manivannan, N.Q. Wu, Effects of pore structure on performance of an activated-carbon supercapacitor electrode recycled from scrap waste tires, *ACS Sustain. Chem. Eng.* 2 (2014) 1592–1598.
- [13] K. Sun, C.Y. Leng, J.C. Jiang, Q. Bu, G.F. Lin, X.C. Lu, G.Z. Zhu, Microporous activated carbons from coconut shells produced by self-activation using the pyrolysis gases produced from them, that have an excellent electric double layer performance, *New Carbon Mater.* 32 (2017) 451–459.
- [14] T.M. Phuong, D.D. Nguyen, D. Nicholson Do, On the hysteresis loop of argon adsorption in cylindrical pores, *J. Phys. Chem. C* 115 (2011) 4706–4720.
- [15] M.X. Liu, F.L. Zhao, D.Z. Zhu, H. Duan, Y.K. Lv, L.C. Li, L.H. Gan, Ultramicroporous carbon nanoparticles derived from metal-organic framework nanoparticles for high-performance supercapacitors, *Mater. Chem. Phys.* 211 (2018) 234–241.
- [16] Y.J. Cai, Y. Luo, Y. Xiao, X. Zhao, Y.R. Liang, H. Hu, H.W. Dong, L.Y. Sun, Y.L. Liu, M.T. Zheng, Facile synthesis of three-dimensional heteroatom- doped and hierarchical egg-box-like carbons derived from *Moringa oleifera* branches for high-performance supercapacitors, *ACS Appl. Mater. Interfaces* 8 (2016) 33060–33071.
- [17] G.F. Ma, Z.G. Zhang, H. Peng, K.J. Sun, F.T. Ran, Z.Q. Lei, Facile preparation of nitrogen-doped porous carbon for high performance symmetric supercapacitor, *J. Solid State Electrochem.* 20 (2016) 1613–1623.
- [18] Y. Fan, P.F. Liu, B. Zhu, S.F. Chen, K.L. Yao, R. Han, Microporous carbon derived from acacia gum with tuned porosity for high-performance electrochemical capacitors, *Int. J. Hydrog. Energy* 40 (2015) 6188–6196.
- [19] H.M. Luo, Y.Z. Chen, B. Mu, Y.J. Fu, X. Zhao, J.Q. Zhang, Preparation and electrochemical performance of attapulgite/citric acid template carbon electrode materials, *J. Appl. Electrochem.* 46 (2016) 299–307.
- [20] J. Zeng, Q. Cao, B. Jing, X.X. Peng, Hierarchical porous nitrogen doping activated carbon with high performance for supercapacitor electrodes, *RSC Adv.* 6 (2016) 15320–15326.
- [21] L. Cheng, X.L. Li, H.J. Liu, H.M. Xiong, P.W. Zhang, Y.Y. Xia, Carbon-coated Li₄Ti₅O₁₂ as a high rate electrode material for Li-ion intercalation, *J. Electrochem. Soc.* 154 (2007) A692–A697.
- [22] K. Yan, L.B. Kong, Y.H. Dai, M. Shi, K.W. Shen, B. Hu, Y.C. Luo, L. Kang, Design and preparation of highly structure-controllable mesoporous carbons at the molecular level and application as electrode materials for supercapacitors, *J. Mater. Chem. A* 3 (2015) 22781–22793.
- [23] Y.M. Tan, C.F. Xu, G.X. Chen, Z.H. Liu, M. Ma, Q.J. Xie, N.F. Zheng, S.Z. Yao, Synthesis of ultrathin nitrogen-doped graphitic carbon nanocages as advanced electrode materials for supercapacitor, *ACS Appl. Mater. Interfaces* 5 (2013) 2241–2248.
- [24] B. Sakintuna, Y. Yürüm, Preparation and characterization of mesoporous carbons using a Turkish natural zeolitic template/furfuryl alcohol system, *Microporous Mesoporous Mater.* 93 (2006) 304–312.
- [25] S.Q. Xiong, J.C. Fan, Y. Wang, J. Zhu, J.R. Yu, Z.M. Hu, A facile template approach to nitrogen-doped hierarchical porous carbon nanospheres from polydopamine for high-performance supercapacitors, *J. Mater. Chem. A* 5 (2017) 18242–18252.
- [26] H. Peng, G.F. Ma, K.J. Sun, J.J. Mu, Z. Zhang, Z.Q. Lei, Formation of carbon nanosheets via simultaneous activation and catalytic carbonization of macroporous anion-exchange resin for supercapacitors application, *ACS Appl. Mater. Interfaces* 6 (2014) 20795–20803.
- [27] X.H. Xia, Y.Q. Zhang, Z.X. Fan, D.L. Chao, Q.Q. Xiong, J.P. Tu, H. Zhang, J.F. Hong, Novel metal@carbon spheres core-shell arrays by controlled self-assembly of carbon nanospheres: a stable and flexible supercapacitor electrode, *Adv. Energy Mater.* 5 (2015) 1401701–1401709.
- [28] T. Tooming, T. Thomberg, H. Kurig, A. Jänes, E. Lust, High power density supercapacitors based on the carbon dioxide activated d-glucose derived carbon electrodes and 1-ethyl-3-methylimidazolium tetrafluoroborate ionic liquid, *J. Power Sources* 280 (2015) 667–677.
- [29] J. Deng, T.Y. Xiong, X. Fan, M.M. Li, C.L. Han, Y.T. Gong, H.Y. Wang, Y. Wang, Inspired by bread leavening: one-pot synthesis of hierarchically porous carbon for supercapacitors, *Green Chem.* 17 (2015) 4053–4060.
- [30] K.T. Cho, B.L. Sang, J.W. Lee, Facile synthesis of highly electrocapacitive nitrogen-doped graphitic porous carbons, *J. Phys. Chem. C* 118 (2014) 9357–9367.